

Designing a compact cavity-enhanced source of entangled photons

Žiga Pušavec

Faculty for Mathematics and Physics, University of Ljubljana, Jadranska 19, 1000 Ljubljana, Slovenia

Lara Ulčakar

*Faculty for Mathematics and Physics, University of Ljubljana, Jadranska 19, 1000 Ljubljana, Slovenia and
Jozef Stefan Institute, Jamova 39, 1000 Ljubljana, Slovenia*

Rainer Kaltenbaek*

*Faculty for Mathematics and Physics, University of Ljubljana, Jadranska 19, 1000 Ljubljana, Slovenia and
Institute for Quantum Optics and Quantum Information,
Austrian Academy of Sciences, Boltzmanngasse 3, 1090 Vienna, Austria*

Quantum repeaters will require sources of entanglement allowing efficient coupling to quantum memories. Here, we address this challenge with a compact, narrowband source design. The entangled pairs are generated via SPDC in two perpendicularly oriented nonlinear crystals in a Fabry-Pérot cavity. We show that the case of highly non-degenerate wavelengths and type-II phase matching is the most promising candidate for a practical implementation. Using the parameters of an experiment we are currently working on, this design should allow generating entangled photons with a bandwidth of a few MHz.

PACS numbers: 03.65.Ud, 03.67.Hk, 03.65.Ud, 42.50.Pq, 42.50.-p, 42.79.Gn

Large-scale quantum networks will use entanglement as a resource for future quantum applications [1, 2]. Establishing such networks is a challenge due to the losses in the optical links connecting the individual nodes. The distribution of entanglement has been demonstrated successfully over a few hundred kilometers in optical fiber networks [3, 4]. Using optical satellite links allows for the distribution over even larger distances, but at the cost of significant losses [5–7]. In optical fibre networks, the range achievable for entanglement distribution can be increased by using quantum repeaters [8]. These combine entanglement distillation and purification [9–11] with entanglement swapping [12] to distribute high-fidelity entanglement over large distances. To avoid exponential loss, the entanglement needs to be stored efficiently until the intermediate steps have been completed successfully [9].

Using narrowband sources of entanglement is beneficial for several purposes. It can increase the efficiency of storing entangled photons in quantum memories [13, 14] and it can reduce the background in the day-light operation of free-space links [7, 15]. Moreover, using narrowband modes allows for frequency division multiplexing. This can increase the bandwidth of quantum channels and allows the simultaneous connection of multiple network clients [3]. Generating narrowband photons can be achieved using cavity-enhanced spontaneous parametric downconversion (SPDC) [16, 17]. Other methods include spontaneous four-wave mixing in hot atomic vapor cells [18, 19] or using laser-cooled atoms [20, 21]. Recent works showed the generation of photon pairs compatible

with the storage in atom-based quantum memories [22–24] and in solid-state quantum memories [25, 26]. In some cases, the actual storage of single photons in quantum memories has already been achieved [27–29].

Generating entanglement, however, requires making two biphoton processes indistinguishable. For example, by exciting indistinguishable processes in a single SPDC crystal [30], or by creating a superposition of two-photon amplitudes originating in multiple crystals [31, 32]. Alternatively, the amplitudes can originate from multiple branches in an interferometer [33]. Recently, there has been significant progress in simultaneously achieving entanglement and narrow bandwidth of the generated photons. In Ref. [34], the light from two cavity-enhanced SPDC crystals was used to generate entanglement with sub-GHz bandwidth in an interferometric setup. Refs. [29, 35] showed the generation of narrowband entanglement using a frequency comb. These photons then were frequency converted to a wavelength compatible with solid-state quantum memories. The authors of Ref. [36] used a single crystal in a bi-directionally pumped bow-tie cavity to generate entangled photons compatible with a $^{40}\text{Ca}^+$ quantum memory.

Here, we present the design of a compact, cavity-enhanced SPDC source of entangled photons without the need for complex interferometric or cavity setups. We will consider realistic experimental parameters to investigate the feasibility of achieving narrowband entanglement using a comparatively simple design. The source (Fig. 1) is based on a single cavity that contains two nonlinear crystals rotated by 90 degrees relative to each other, inspired by [16, 37–39]. The crystals can be of different lengths, l_1 and l_2 . We pump the crystals with light at frequency ω_p and with the polarization chosen to balance the brightness of both SPDC processes.

* rainer.kaltenbaek@fmf.uni-lj.si

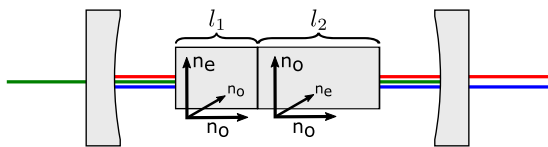


FIG. 1. Schematic of two nonlinear crystals of lengths l_1 and l_2 in a Fabry Perot cavity. The green line indicates the pump beam, the blue and red lines indicate the signal and idler photons generated by SPDC. The optical axes of the crystals are mutually orthogonal.

Depending on its polarization, the pump photon will create a pair of SPDC photons in the first or the second crystal. These photons are denoted as the signal and the idler with frequencies ω_s and ω_i , respectively. Like the crystal axes, the polarization directions of the photons created in the first crystal will be perpendicular to those created in the second crystal.

Since the pump photon can generate an SPDC pair either in the first or in the second crystal, the corresponding two-photon state will be a linear combination of these two processes:

$$|\psi\rangle = \frac{1}{\sqrt{2}} \left(a_1^\dagger(\omega_s) a_2^\dagger(\omega_i) + e^{i\varphi} a_3^\dagger(\omega_i) a_4^\dagger(\omega_s) \right) |\text{vac}\rangle. \quad (1)$$

φ is a relative phase and $a_n^\dagger(\omega)$ is a boson creation operator of mode j at frequency ω . j can indicate the polarization or the crystal of origin. The polarization of the photons generated is determined by the PM condition. For type-II SPDC, the state will be a superposition of the Bell states $|\psi^\pm\rangle$, while it will be a superposition of Bell states $|\Phi^\pm\rangle$ for type-0 and type-I SPDC [40]. If the signal and idler photons originate from type-II SPDC and have degenerate frequencies, the amplitudes from different crystals will result in a product state $a_H^\dagger(\omega) a_V^\dagger(\omega) (1 + e^{i\varphi}) |\text{vac}\rangle$. Using our source design with type-II PM to generate entanglement is therefore not possible for degenerate frequencies. For type-0 and type-I SPDC, one cannot spatially separate the photons if the frequencies are degenerate. For these reasons, we will focus on two specific cases: (1) the photons produced have *near*-degenerate wavelengths suitable for the low-loss distribution in telecommunication fibers, (2) only one photon is at such a telecommunication wavelength, and the second one has a wavelength suitable for efficiently coupling to a quantum memory.

Typically, the bandwidth of SPDC photons is much broader than the acceptance bandwidth of quantum memories [13, 14]. The effective bandwidth can be reduced by coupling the process to an optical cavity [16, 22, 39, 41]. Only the portions of the photon spectra that are resonant with the narrow cavity modes will be enhanced. In comparison, the remainder of the spectra will be strongly suppressed. For each mode, denoted by an index j , we can define the mode number m_j , which is the phase shift that light in mode j acquires during one cavity round trip. For example, in the case of a

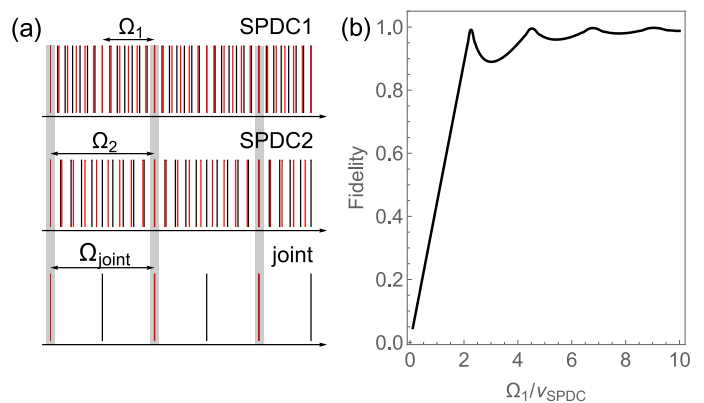


FIG. 2. (a) Illustration of the cluster spacings of double resonances and the joint cluster spacing for quadruple resonances. Red and black lines indicate idler and signal resonances, respectively. The upper segment shows the occurrence of double resonances for SPDC in the first crystal, the middle segment for SPDC in the second crystal. The bottom segment shows the occurrence of double resonances for both crystals, and the gray-shaded area highlights the occurrence of quadruple resonances, where the signal and idler modes from both SPDC processes are resonant simultaneously. (b) The fidelity of the state of a photon pair from a single crystal in well-defined frequency modes as a function of the cluster spacing normalized to the SPDC bandwidth.

two-crystal type-II source, the four corresponding mode numbers are:

$$\begin{aligned} m_1(\omega_s) &= \frac{\omega_s}{\pi c} (l_1 n_o(\omega_s) + l_2 n_e(\omega_s) + l_{\text{air}}), \\ m_2(\omega_i) &= \frac{\omega_i}{\pi c} (l_1 n_e(\omega_i) + l_2 n_o(\omega_i) + l_{\text{air}}), \\ m_3(\omega_s) &= \frac{\omega_s}{\pi c} (l_1 n_e(\omega_s) + l_2 n_o(\omega_s) + l_{\text{air}}), \\ m_4(\omega_i) &= \frac{\omega_i}{\pi c} (l_1 n_o(\omega_i) + l_2 n_e(\omega_i) + l_{\text{air}}). \end{aligned} \quad (2)$$

Here, m_1 and m_2 represent the downconverted signal and idler mode numbers originating in the first crystal, while m_3 and m_4 represent the equivalent mode numbers for the second crystal. A single mode j is resonant with the cavity if its frequency is an integer multiple of the free spectral range $\text{FSR}_j = |\partial_\omega m_j|^{-1} / 2\pi$. Here, ∂_ω denotes the partial derivative with respect to ω . To achieve narrowband entanglement between photons in these four modes, all of them have to be resonant with the cavity simultaneously. We denote this as a quadruple resonance.

Due to the frequency-dependent birefringence of the crystals, and due to their different lengths, the FSRs of the downconverted modes will be different. Simultaneous resonances of multiple modes will occur only at specific frequency spacings much greater than individual FSRs. This is known as cluster spacing. The cluster spacing Ω_1 of a double resonance between modes 1 and 2 can be

expressed in terms of their FSRs [16, 39]:

$$\Omega_1 = \frac{\text{FSR}_1 \text{FSR}_2}{|\text{FSR}_1 - \text{FSR}_2|}. \quad (3)$$

Similarly, the cluster spacing Ω_2 is calculated for the modes 3 and 4. For quadruple resonances, we define the joint cluster spacing Ω_{joint} by replacing FSR_1 and FSR_2 in Eq. 3 with Ω_1 and Ω_2 , respectively. Fig. 2(a) illustrates this relationship.

One wants to have the joint cluster spacing small enough such that finding a quadruple resonance is achievable by tuning control parameters within a parameter range that is experimentally feasible. An additional challenge is finding the right ratio between the cluster spacing and the SPDC bandwidth. If the cluster spacing in an individual crystal is smaller than the corresponding SPDC bandwidth, multiple cavity modes at different frequencies will be enhanced. The output state of the cavity-enhanced SPDC in crystal α will then be a linear combination of these modes: $\sum_j A_j^\alpha a_1^\dagger(\omega_s + j\Omega_\alpha) a_2^\dagger(\omega_i - j\Omega_\alpha) |\text{vac}\rangle$. Here, $A_j^\alpha = \text{sinc}(l_\alpha \Delta k_j / 2)$ are normalized amplitudes depending on the phase mismatch of the SPDC process Δk_j (see Appendix A). $\alpha = 1, 2$ denotes crystal 1 or 2. Fig. 2(b) shows the calculated fidelity of the output state of crystal 1 for type-II PM with a product state $a_H^\dagger(\omega_s) a_V^\dagger(\omega_i) |\text{vac}\rangle$ as a function of cluster spacing normalized to the SPDC bandwidth. The plot shows that a fidelity larger than 0.9 is achieved for

$$\Omega / \Delta \nu_{\text{SPDC}} > 2. \quad (4)$$

This gives us a target bound for the source design if no additional spectral filtering is used.

In the following, we will assume realistic experimental parameters and analyze the feasibility of the source design for the cases of near-degenerate and highly non-degenerate frequencies using type-0 and type-II PM. For the SPDC crystals, we assume 5% MgO-doped periodically poled Lithium Niobate (PPLN) due to its high non-linearity and transparency at 1550 nm [42].

First, let us consider a near-degenerate source. We assume a pump wavelength of 775 nm and near-degenerate signal and idler modes at 1550 nm $\pm \Delta\lambda/2$. $\Delta\lambda$ corresponds to a small frequency shift $\Delta\omega = 2\pi \times 80$ MHz. Fig. 3(a) shows the SPDC bandwidth and the cluster spacing of the modes originating in crystal 1 for type-II and type-0 PM, as a function of the joint crystal length [43]. For type-0 SPDC, the bandwidth and the cluster spacing are exceedingly high, whereas for type-II SPDC, the SPDC bandwidth is notably less than the cluster spacing. This means that a source based on type-0 PM is not possible but a setup based on type-II may be feasible. In particular, using type-II PM can ensure that cavity enhancement is achieved for the intended single pair of frequencies with high fidelity.

Generating entangled pairs, however, requires a quadruple resonance, and we will see in the following that this is not possible for a near-degenerate source even for

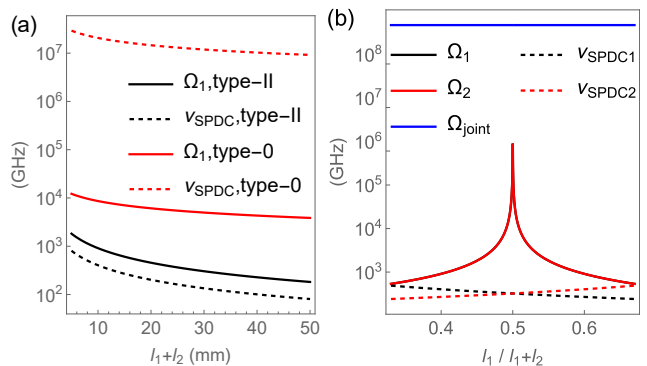


FIG. 3. Cluster spacings vs SPDC bandwidths in the C-band at near-degenerate wavelengths centered around 1550 nm with a frequency difference of 80 MHz. (a) Comparison of type-II and type-0 phase matching (PM) when creating photon pairs in a single crystal. The dashed lines show the bandwidths of the SPDC processes, the solid lines show the corresponding cluster spacings as a function of the joint crystal length $l_1 + l_2$ at a fixed ratio $l_1 / (l_1 + l_2) = 0.4$. Because the SPDC bandwidth is larger than the cluster spacing, type-0 PM does not allow generating photon pairs of well-defined frequencies. (b) Comparing the joint cluster spacing to the individual cluster spacings and the SPDC bandwidths in the two crystals for type-II PM. We plot them as a function of the ratio of crystal lengths for a fixed joint crystal length $l_1 + l_2 = 10$ mm. The joint cluster spacing for type-II PM is too large to allow finding a quadruple resonance under realistic conditions.

type-II PM. Fig. 3(b) shows that the cluster spacings of the double resonances grow significantly as the ratio of $l_1 / (l_1 + l_2)$ approaches 0.5. At this point, the four crystal modes nearly become degenerate for small $\Delta\omega$. One can see that the joint cluster spacing is extremely large for all length ratios. Two quadruple resonances would be displaced by a wavelength shift of more than $1 \mu\text{m}$. A type-II near-degenerate source could therefore produce narrowband photon pairs, but an entangled state cannot be achieved since one cannot find a quadruple resonance in practice.

Secondly, let us consider the case of a highly non-degenerate source. We assume a pump wavelength of 519 nm to generate signal photons at the Rubidium transition $\lambda_s = 780.24$ nm and idler photons at $\lambda_i = 1550$ nm.

Fig. 4(a) shows the SPDC bandwidth and the cluster spacing of a double resonance in crystal 1 as a function of the joint crystal length. Note that both the cluster spacing and the SPDC bandwidth reduce as the crystal length increases. For both types of phase matching, the SPDC bandwidth is too large to generate photon pairs where the frequency of each individual photon is well defined. The corresponding fidelity will therefore be only 0.5 for a type-II source and 0.2 for a type-0 source (see Fig. 2(b)). Type-0 PM has the additional disadvantage that the joint cluster spacing is on the order of THz (see Appendix B). This makes it impossible to find the quadruple resonances necessary for generating entangled photon pairs.

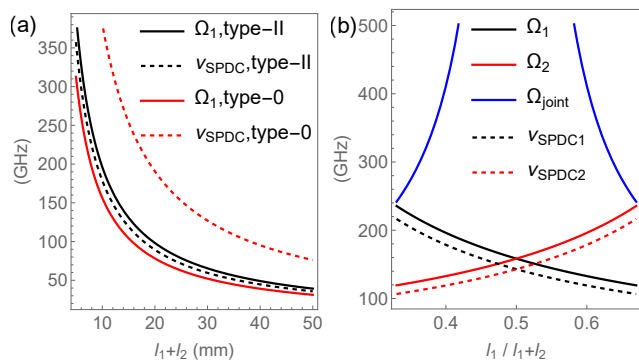


FIG. 4. Cluster spacings vs SPDC bandwidths for highly non-degenerate wavelengths $\lambda_i = 780.24$ nm and $\lambda_s = 1550$ nm. (a) Comparison of type-II and type-0 phase matching (PM) when creating photon pairs in a single crystal. The dashed lines show the bandwidths of the SPDC processes, the solid lines show the corresponding cluster spacings as a function of the joint crystal length $l_1 + l_2$ at a fixed ratio $l_1 / (l_1 + l_2) = 0.4$. As in Fig. 3, the SPDC bandwidth is larger than the cluster spacing for type-0 PM. Therefore, type-II PM is more suitable for generating photon pairs of well-defined frequencies. (b) Comparing the joint cluster spacing to the individual cluster spacings and the SPDC bandwidths in the two crystals for type-II PM. We plot them as a function of the ratio of crystal lengths for a fixed joint crystal length $l_1 + l_2 = 10$ mm. In contrast to Fig. 3, there is a range of crystal length ratios (between 0.3 and 0.4), where the joint cluster spacing does not diverge but is still sufficiently large compared to the individual cluster spacings and SPDC bandwidths to create high-fidelity entanglement.

We will therefore focus on finding quadruple resonances for the more favorable type-II PM. To achieve that, we investigate the dependence of the joint cluster spacing on the ratio of the crystal lengths as shown in Fig. 4(b). If the crystal lengths are the same, the joint cluster spacing will diverge since the two pairs of cavity modes become identical and will have the same cluster spacing for double resonances. To allow finding a quadruple resonance to generate entangled states, we therefore choose crystals of differing lengths. Even then, the SPDC processes in the individual crystals can still produce photons in multiple frequency modes.

One solution is to introduce additional filtering of the cavity output. The practicality of this solution will depend on the spacing of the double resonances. Alternatively, one can introduce a relative optical path delay Δl to idler modes 2 and 4 while keeping the signal modes unchanged. We model this path delay by adding

$\Delta l \omega_i / \pi c$ to $m_{2/4}$. This will leave the SPDC bandwidths and the joint cluster spacing unchanged, but it will affect the cluster spacings for the SPDC processes in the individual crystals. Using this approach and $\Delta l = 550$ μm , one can achieve a fidelity of 0.93 of the state generated with the targeted polarization entangled state as in Eq. 1 (see Appendix D).

The bandwidth of the state the source will generate depends on the cavity linewidth, which is determined by the intracavity losses and the cavity length. To provide a numeric estimate, let us assume the nonlinear crystals to be PPLN with a joint crystal length of 10 mm. This will determine the optimal length of the cavity (53 mm) in reference to the focusing parameter [41]. For mirror reflectivities of 99.98%, achieving a bandwidth of 1 MHz will require a finesse of 3000. This gives an upper boundary of 0.2% for the intracavity losses. Achieving such low losses is possible by picking appropriate anti-reflection coatings for PPLN. For additional details, see Appendix E.

We presented a design for a compact cavity-enhanced source of polarization-entangled photons. The photon pairs are generated in two nonlinear crystals with perpendicular optical axes inside a single Fabry-Pérot cavity. We studied the feasibility of the design for different types of phase matching and for near-degenerate as well as highly non-degenerate wavelengths. The combination of type-II phase matching and highly-nondegenerate wavelengths should allow the generation of high-fidelity narrowband entangled photon pairs for realistic experimental parameters. The presented design is the basis for an experimental realization we are currently working on. In addition to the considerations presented here, an actual implementation will require a high-precision control of experimental parameters to find and actively stay on the necessary quadruple resonance of the cavity. This will include the stabilization of the crystal temperatures, the cavity length, and the pump wavelength.

ACKNOWLEDGMENTS

ŽP and RK acknowledge support by the Slovenian Research Agency under contracts no. J2-2514, N1-0180, P1-0416, J1-9145, P1-0125. LU acknowledges funding by the Slovenian Research Agency under contracts no. J1-2458 and P1-0416. All authors were supported by the Republic of Slovenia (MVZI) and the European Union - NextGenerationEU (SiQUID-101091560).

-
- [1] R. Horodecki, P. Horodecki, M. Horodecki, and K. Horodecki, *Reviews of Modern Physics* **81**, 865 (2009), publisher: American Physical Society.
 [2] S. Wehner, D. Elkouss, and R. Hanson, *Science* **362** (2018), 10.1126/science.aam9288, publisher: American

Association for the Advancement of Science Section: Review.

- [3] S. P. Neumann, A. Buchner, L. Bulla, M. Bohmann, and R. Ursin, *Nature Communications* **13** (2022), 10.1038/s41467-022-33919-0.

- [4] S.-C. Zhuang, B. Li, M.-Y. Zheng, Y.-X. Zeng, H.-N. Wu, G.-B. Li, Q. Yao, X.-P. Xie, Y.-H. Li, H. Qin, L.-X. You, F.-H. Xu, J. Yin, Y. Cao, Q. Zhang, C.-Z. Peng, and J.-W. Pan, “Ultrabright-entanglement-based quantum key distribution over a 404-km-long optical fiber,” (2024), arXiv:2408.04361 [quant-ph].
- [5] J. Yin, Y. Cao, Y.-H. Li, S.-K. Liao, L. Zhang, J.-G. Ren, W.-Q. Cai, W.-Y. Liu, B. Li, H. Dai, G.-B. Li, Q.-M. Lu, Y.-H. Gong, Y. Xu, S.-L. Li, F.-Z. Li, Y.-Y. Yin, Z.-Q. Jiang, M. Li, J.-J. Jia, G. Ren, D. He, Y.-L. Zhou, X.-X. Zhang, N. Wang, X. Chang, Z.-C. Zhu, N.-L. Liu, Y.-A. Chen, C.-Y. Lu, R. Shu, C.-Z. Peng, J.-Y. Wang, and J.-W. Pan, *Science* **356**, 1140 (2017).
- [6] J. S. Sidhu, S. K. Joshi, M. Gündoğan, T. Brougham, D. Lowndes, L. Mazzarella, M. Krutzik, S. Mohapatra, D. Dequal, G. Vallone, P. Villoresi, A. Ling, T. Jennewein, M. Mohageg, J. G. Rarity, I. Fuentes, S. Pirandola, and D. K. L. Oi, *IET Quantum Communication* **2**, 182 (2021), eprint: <https://onlinelibrary.wiley.com/doi/pdf/10.1049/qtc2.12015>.
- [7] A. Kržič, S. Sharma, C. Spiess, U. Chandrashekhara, S. Töpfer, G. Sauer, L. J. González-Martín del Campo, T. Kopf, S. Petschornig, T. Grafenauer, R. Lieger, B. Ömer, C. Pacher, R. Berlich, T. Peschel, C. Damm, S. Risse, M. Goy, D. Rieländer, A. Tünnermann, and F. Steinlechner, *npj Quantum Information* **9**, 1 (2023), publisher: Nature Publishing Group.
- [8] H.-J. Briegel, W. Dür, J. I. Cirac, and P. Zoller, *Phys. Rev. Lett.* **81**, 5932 (1998).
- [9] C. H. Bennett, G. Brassard, S. Popescu, B. Schumacher, J. A. Smolin, and W. K. Wootters, *Phys. Rev. Lett.* **76**, 722 (1996).
- [10] D. Deutsch, A. Ekert, R. Jozsa, C. Macchiavello, S. Popescu, and A. Sanpera, *Physical Review Letters* **77**, 2818 (1996), publisher: American Physical Society.
- [11] W. K. Wootters, *Physical Review Letters* **80**, 2245 (1998), publisher: American Physical Society.
- [12] M. Żukowski, A. Zeilinger, M. A. Horne, and A. K. Ekert, *Phys. Rev. Lett.* **71**, 4287 (1993).
- [13] Y. Wang, J. Li, S. Zhang, K. Su, Y. Zhou, K. Liao, S. Du, H. Yan, and S.-L. Zhu, *Nature Photonics* **13**, 346 (2019), publisher: Nature Publishing Group.
- [14] L. Heller, J. Lowinski, K. Theophilo, A. Padrón-Brito, and H. de Riedmatten, *Physical Review Applied* **18**, 024036 (2022), publisher: American Physical Society.
- [15] M. Aspelmeyer, H. R. Böhm, T. Gyatso, T. Jennewein, R. Kaltenbaek, M. Lindenthal, G. Molina-Terriza, A. Poppe, K. J. Resch, M. Taraba, R. Ursin, P. Walther, and A. Zeilinger, *Science* **301**, 621 (2003).
- [16] C.-S. Chuu, G. Y. Yin, and S. E. Harris, *Applied Physics Letters* **101**, 051108 (2012).
- [17] A. Lenhard, M. Bock, C. Becher, S. Kucera, J. Brito, P. Eich, P. Müller, and J. Eschner, *Physical Review A* **92**, 063827 (2015), publisher: American Physical Society.
- [18] L. Zhu, X. Guo, C. Shu, H. Jeong, and S. Du, *Applied Physics Letters* **110** (2017), 10.1063/1.4980073.
- [19] C.-Y. Hsu, Y.-S. Wang, J.-M. Chen, F.-C. Huang, Y.-T. Ke, E. K. Huang, W. Hung, K.-L. Chao, S.-S. Hsiao, Y.-H. Chen, C.-S. Chuu, Y.-C. Chen, Y.-F. Chen, and I. A. Yu, *Optics Express* **29**, 4632 (2021).
- [20] Y.-S. Wang, K.-B. Li, C.-F. Chang, T.-W. Lin, J.-Q. Li, S.-S. Hsiao, J.-M. Chen, Y.-H. Lai, Y.-C. Chen, Y.-F. Chen, C.-S. Chuu, and I. A. Yu, *APL Photonics* **7**, 126102 (2022).
- [21] A. Bruns, C.-Y. Hsu, S. Stryzhenko, E. Giese, L. P. Yatsenko, I. A. Yu, T. Halfmann, and T. Peters, *Quantum Science and Technology* **8**, 015002 (2022).
- [22] P.-J. Tsai and Y.-C. Chen, *Quantum Science and Technology* **3**, 034005 (2018).
- [23] V. Prakash, L. C. Bianchet, M. T. Cuairan, P. Gomez, N. Bruno, and M. W. Mitchell, *Optics Express* **27**, 38463 (2019).
- [24] H. He, P.-F. Yang, P.-F. Zhang, G. Li, and T.-C. Zhang, *Frontiers of Physics* **18** (2023), 10.1007/s11467-023-1317-z.
- [25] J. Liu, J. Liu, P. Yu, and G. Zhang, *APL Photonics* **5** (2020), 10.1063/5.0006021.
- [26] R. Onozawa, D. Yoshida, K. Niizeki, and T. Horikiri, *Japanese Journal of Applied Physics* **61**, 102008 (2022).
- [27] K. Mannami, T. Kondo, T. Tsuno, T. Miyashita, D. Yoshida, K. Ito, K. Niizeki, I. Nakamura, F.-L. Hong, and T. Horikiri, *Optics Express* **29**, 41522 (2021).
- [28] G. Buser, R. Mottola, B. Cotting, J. Wolters, and P. Treutlein, *PRX Quantum* **3**, 020349 (2022).
- [29] K. Ito, T. Kondo, K. Mannami, K. Niizeki, D. Yoshida, K. Minaguchi, M. Zheng, X. Xie, F.-L. Hong, and T. Horikiri, *Phys. Rev. Appl.* **19**, 024070 (2023).
- [30] P. G. Kwiat, K. Mattle, H. Weinfurter, A. Zeilinger, A. V. Sergienko, and Y. Shih, *Physical Review Letters* **75**, 4337 (1995), publisher: American Physical Society.
- [31] P. G. Kwiat, E. Waks, A. G. White, I. Appelbaum, and P. H. Eberhard, *Phys. Rev. A* **60**, R773 (1999).
- [32] D. Ljunggren and M. Tengner, *Phys. Rev. A* **72**, 062301 (2005).
- [33] A. Fedrizzi, T. Herbst, A. Poppe, T. Jennewein, and A. Zeilinger, *Optics Express* **15**, 15377 (2007), publisher: Optica Publishing Group.
- [34] M.-Y. Gao, Y.-H. Li, Y. Li, Z. Zhou, G.-C. Guo, Z.-Y. Zhou, and B.-S. Shi, *Phys. Rev. A* **109**, 033720 (2024).
- [35] K. Niizeki, D. Yoshida, K. Ito, I. Nakamura, N. Takei, K. Okamura, M.-Y. Zheng, X.-P. Xie, and T. Horikiri, *Communications Physics* **3**, 138 (2020).
- [36] E. Arenskötter, T. Bauer, S. Kucera, M. Bock, J. Eschner, and C. Becher, *npj Quantum Information* **9** (2023), 10.1038/s41534-023-00701-z.
- [37] D. Ljunggren, M. Tengner, P. Marsden, and M. Pelton, *Phys. Rev. A* **73**, 032326 (2006).
- [38] P. Trojek and H. Weinfurter, *Applied Physics Letters* **92**, 211103 (2008).
- [39] C.-S. Chuu and S. E. Harris, *Phys. Rev. A* **83**, 061803 (2011).
- [40] $|\psi^\pm\rangle = (1/\sqrt{2})(|HV\rangle \pm |VH\rangle)$ and $|\Phi^\pm\rangle = (1/\sqrt{2})(|HH\rangle \pm |VV\rangle)$.
- [41] G. D. Boyd and A. Ashkin, *Phys. Rev.* **146**, 187 (1966).
- [42] O. Gayer, Z. Sacks, E. Galun, and A. Arie, *Applied Physics B* **91**, 343 (2008).
- [43] Type-0 cluster spacing was calculated using a second order expansion, see Appendix C. For the SPDC photons originating in crystal 2, identical considerations can be made.
- [44] D. H. Jundt, *Opt. Lett.* **22**, 1553 (1997).
- [45] R. C. Eckardt, C. D. Nabors, W. J. Kozlovsky, and R. L. Byer, *J. Opt. Soc. Am. B* **8**, 646 (1991).
- [46] N. Ismail, C. C. Kores, D. Geskus, and M. Pollnau, *Opt. Express* **24**, 16366 (2016).
- [47] G. D. Boyd and D. A. Kleinman, *Journal of Applied Physics* **39**, 3597 (1968).

Appendix A: Phase-mismatch and bandwidth

The bandwidth of a single-pass SPDC is determined by the phase mismatch of the nonlinear process $\Delta k = k_s + k_i - k_p - 2\pi/\Lambda$. Here, Λ is the periodic poling of the SPDC crystal. The amplitude of the photons generated in a crystal of length l is proportional to $(\sin \xi/\xi)^2$ with $\xi = \Delta k l/2$. The FWHM bandwidth $\Delta\nu_{\text{SPDC}}$ of the SPDC photons can then be determined from $\xi_{\text{HWHM}} \approx 1.39$. Expanding Δk up to linear order in signal frequency and temperature yields:

$$\Delta k = \left(\frac{\partial \Delta k}{\partial \omega_s} \right)_{\omega_p} \Delta \omega_s + \frac{\partial \Delta k}{\partial T} \Delta T = \frac{2\xi_{\text{HWHM}}}{l}. \quad (\text{A1})$$

Here, T is the crystal temperature, which affects the refractive index and the poling of the nonlinear crystal [42, 44]. The SPDC bandwidth is then determined from the solution of Eq. A1 as $2\omega_s$.

Appendix B: Additional cluster spacing plots

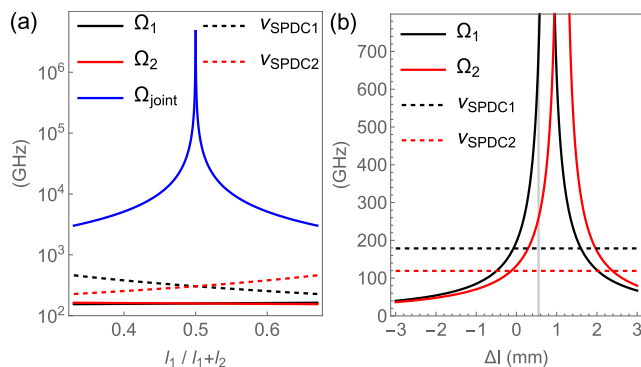


FIG. 5. (a) Cluster spacing as a function of the ratio of crystal lengths for a non-degenerate type-0 source at $\lambda_i = 1550$ nm and the Rubidium transition at $\lambda_s = 780.24$ nm. For all length ratios, the joint cluster spacing is larger than 1 THz, which makes the quadruple resonance essentially impossible to find. (b) Cluster spacing and SPDC bandwidth of a type-2 source at the Rubidium transition at $\lambda_s = 780.24$ nm and for $\lambda_i = 1550$ nm. An additional optical-path delay Δl is added to modes 2 and 4. For $\Delta l = 550 \mu\text{m}$, the cluster spacings of the double resonances from both SPDC processes become twice as large as the corresponding SPDC bandwidths. For these values, one can achieve a fidelity of 0.93 with the targeted maximally entangled state $|\psi^-\rangle$.

Appendix C: Cluster spacing using higher-order approximations

In the main text, we used a linear approximation for calculating the cluster spacing. For most of the cases we considered there, this approximation yields the same

results as a more detailed, higher-order calculation. The latter uses the definition of cluster spacing by Eckardt et al [45]. They found that the sum of two mode numbers $m = m_1 + m_2$ will always be very close to an integer value if one is on a double resonance. This results from the fact that the sum of the signal and idler frequencies has to be equal to the pump frequency.

The cluster spacing Ω can then be determined from an integer change in the joint mode number:

$$\Delta m = \pm 1. \quad (\text{C1})$$

Apart from the frequencies of the optical modes involved, the cluster spacing can also depend on other system parameters. To take this into account, Eckert et al [45] expand the joint mode number to second order in frequency and to first order in other parameters like, e.g., the crystal temperature T :

$$\Delta m = \left(\frac{\partial m}{\partial \omega_j} \right)_{\omega_p} \Omega + \frac{1}{2} \left(\frac{\partial^2 m}{\partial \omega_j^2} \right)_{\omega_p} \Omega^2 + \left(\frac{\partial m}{\partial T} \right) (T - T_0). \quad (\text{C2})$$

Using the following relation resulting from energy conservation:

$$\left(\frac{\partial f}{\partial \omega_s} \right)_{\omega_p} = \frac{\partial f}{\partial \omega_s} - \frac{\partial f}{\partial \omega_i}, \quad (\text{C3})$$

one can calculate the partial derivatives occurring in Eq. C2:

$$\begin{aligned} \left(\frac{\partial m}{\partial \omega_s} \right)_{\omega_p} &= \frac{\partial m_1(\omega_s)}{\partial \omega_s} - \frac{\partial m_2(\omega_i)}{\partial \omega_i}, \\ \left(\frac{\partial^2 m}{\partial \omega_s^2} \right)_{\omega_p} &= \frac{\partial^2 m_1(\omega_s)}{\partial \omega_s^2} + \frac{\partial^2 m_2(\omega_i)}{\partial \omega_i^2}. \end{aligned} \quad (\text{C4})$$

The cluster spacing can be calculated by solving Eq. C1. This yields four possible solutions. We consider the solution yielding the lowest cluster spacing frequency because this determines the distance to the next closest cluster. In Fig. 6, we provide a comparison of the cluster spacing using the linear approximation of Eq. 3 in the main text and the cluster spacing derived from integer changes of the joint mode number. One can see deviations between the solutions for the first and second-order approximations close to parameters where the cluster spacing diverges. Examples are the case of a near-degenerate source close to equal crystal lengths ($l_1 \approx l_2$) and the case of non-degenerate frequencies at $l_1 \rightarrow 0$.

Appendix D: The fidelity with the target Bell state

In order to quantify the quality of the state produced by the source, we calculate its fidelity with the

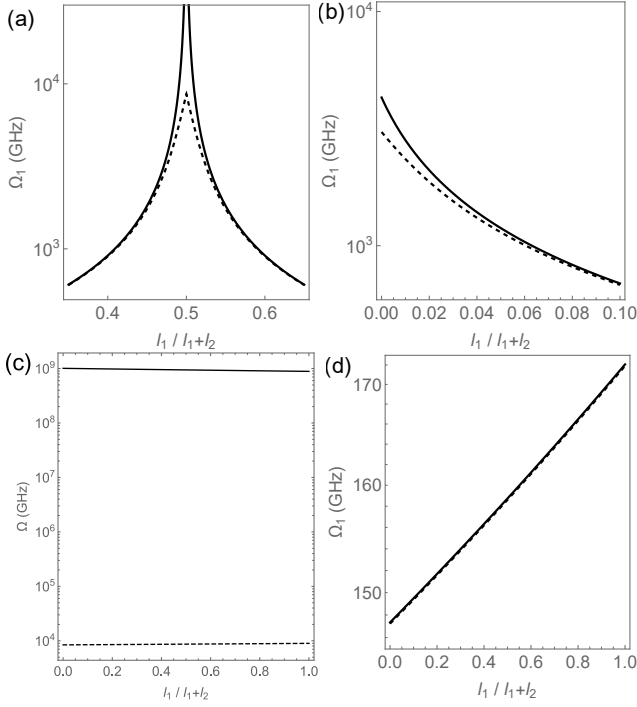


FIG. 6. Comparison of the values for the cluster spacing determined using the first-order (solid) and the second-order approximation (dashed). The left-hand panels are for the near-degenerate wavelengths centered around 1550 nm with a frequency difference of 80 MHz. The right-hand panels are for the strongly non-degenerate case of wavelengths 780.24 nm and 1550 nm. The top panels are for type-II phase matching (PM), the bottom ones are for type-0 PM. We assumed a joint crystal length of $l_1 + l_2 = 10$ mm. This shows that the first and the second-order approximation only differ significantly for near-degenerate PM: either for type-II PM and near-identical crystal lengths, or for type-0 PM.

polarization-entangled Bell state we target. Here, we will assume $|\psi^-\rangle$. The biphotons generated will be a superposition of two-photon amplitudes of SPDC processes in crystal 1 and 2 for all possible frequency combinations of signal and idler photons within the SPDC bandwidth. These amplitudes will only couple efficiently to a cavity mode if the respective frequencies are resonant with the cavity. For type-II phase matching, we can write the two-photon state as:

$$|\Psi\rangle = \sum_{j=-\infty}^{\infty} \left(A_j^1 a_H^\dagger(\omega_s + j\Omega_1) a_V^\dagger(\omega_i - j\Omega_1) + A_j^2 a_V^\dagger(\omega_s + j\Omega_2) a_H^\dagger(\omega_i - j\Omega_2) \right) |\text{vac}\rangle. \quad (\text{D1})$$

Here, we assume that ω_s and ω_i both are resonant with the cavity. The amplitude for a given combination of signal and idler frequencies to the overall state is given by the normalized amplitude $A_j^\alpha = \text{sinc}(l_\alpha \Delta k_{j,\alpha}/2)$ of the SPDC process at that frequency. The index $\alpha = 1, 2$ denotes whether the SPDC process is happening in the first or the second crystal. If there is only one crystal

as in the example in the main text, one can drop the index α and write Δk_j instead. To first order, the phase mismatch is equal to:

$$\Delta k_{j,\alpha} \approx \frac{j\Omega_\alpha}{c} \left(-n_{o/e}(\omega_s) - \omega_s \left(\frac{\partial n_{o/e}}{\partial \omega} \right)_{\omega_s} + n_{e/o}(\omega_i) + \omega_i \left(\frac{\partial n_{e/o}}{\partial \omega} \right)_{\omega_i} \right). \quad (\text{D2})$$

The pump polarization is chosen such that the absolute values of the amplitudes for the central frequencies are equal ($|A_0^1| = |A_0^2|$), and that their relative phase matches that of the target Bell state. For example, $A_0^1 = -A_0^2$ for $|\psi^-\rangle$. All of the other frequency contributions with $n \neq 0$ lower the fidelity with the targeted Bell state, $F = |\langle \Psi | \psi^\pm \rangle|^2$.

Appendix E: The minimum linewidth in a cavity

The goal of the present paper has been to describe the design of a source of entangled photons allowing efficient coupling to quantum memories. This coupling efficiency will be better the narrower the photon bandwidth. However, that bandwidth has to balance two contrary needs: a high rate of entangled pairs to overcome losses and a good coupling efficiency to quantum memories. Here, we assume a bandwidth of 1 MHz to be a reasonable compromise. For example, this will allow good coupling to Rb quantum memories [13, 23].

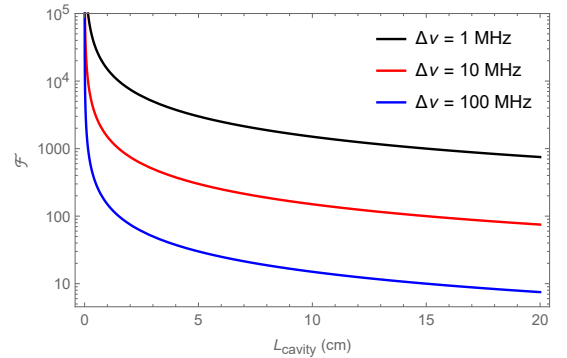


FIG. 7. The finesse required to achieve a specific cavity linewidth as a function of the cavity length.

The bandwidth achievable for the photon pairs produced will be determined by the properties of the cavity. In particular, it is related to the finesse, which is defined as:

$$\mathcal{F} = \frac{\text{FSR}}{\Delta\nu}, \quad (\text{E1})$$

where $\Delta\nu$ is the FWHM linewidth of the cavity, and $\text{FSR} = c/2L_{\text{cavity}}$. The dependence of the finesse on the cavity length L_{cavity} and its relation to the cavity linewidth are shown in Fig. 7. Of course, increasing the

cavity length too much will contradict our goal of building a compact source of entangled photons.

To keep the source as compact as possible, one has to find other means of increasing the cavity finesse. The finesse depends on the mirror reflectivities R_1 and R_2 and the intracavity losses η in the following way:

$$\mathcal{F} = \pi \arccos \left(\frac{4\sqrt{R_1 R_2 (1 - \eta)} - R_1 R_2 (1 - \eta) - 1}{2\sqrt{R_1 R_2 (1 - \eta)}} \right)^{-1}. \quad (\text{E2})$$

A derivation of an equivalent expression for the finesse can be found in Ref. [46]. Increasing the finesse can be achieved by choosing high reflectivities for the cavity mirrors, high-quality antireflection coatings for the crystal end faces and low-absorption nonlinear crystals.

Let us now estimate an upper limit on the reflectivities of the antireflection coating for the wavelengths of the SPDC photons. To this end, we fix the two mirror reflectivities to be the same ($R_1 = R_2 \equiv R$) and then calculate the linewidth as a function of the corresponding intra-cavity losses using Eq. (E1). & (E2). In Fig. 8, this dependence is shown for a 1 cm long PPLN crystal and for several choices of mirror reflectivities. We neglected the losses in PPLN compared to the losses due to the anti-reflection coatings. The cavity length is de-

termined by first finding the optimal focusing condition [47] and then matching the curvature of the optimally focused beam to the curvature of the cavity mirrors, which we assume to be 15 mm. By also taking into account the refractive index of PPLN, we get an effective cavity length of 53 mm.

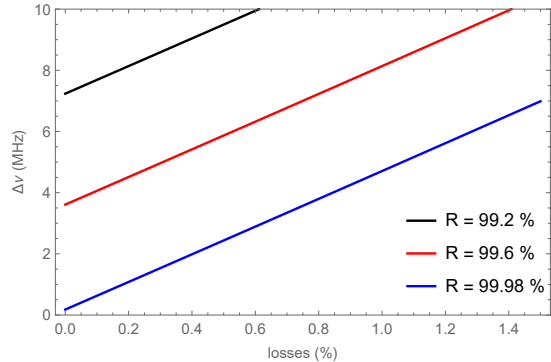


FIG. 8. The dependence of the cavity linewidth on the intracavity losses for specific reflectivities of the cavity mirrors. The cavity length is 53 mm.